Eur J Nucl Med Mol Imaging (2007) 34:1388–1395
DOI 10.1007/s00259-006-0351-8

ORIGINAL ARTICLE

Individual voxelwise dosimetry of targeted ^{90}Y-labelled substance P radiotherapy for malignant gliomas

Stefan Kneifel · Peter Bernhardt · Helena Uusijärvi · Stephan Good · Ludwig Plasswilm · Carlos Buitrago-Téllez · Jan Müller-Brand · Helmut Mäcke · Adrian Merlo

Received: 15 April 2005 / Accepted: 17 November 2006 / Published online: 31 January 2007

Abstract
Purpose Substance P is the main ligand of neurokinin type 1 (NK-1) receptors, which are consistently overexpressed in malignant gliomas. The peptidic vector ^{111}In/^{90}Y-DOTAGA-substance P binds to these receptors and can be used for local treatment of brain tumours. Dosimetry for this interstitial brachytherapy has mainly been done using geometrical models; however, they often do not faithfully reproduce the in vivo biodistribution of radiopharmaceuticals, which is indispensable to correlate the deposited energy with clinical response. The aim of this study was to establish a reproducible dosimetry protocol for intratumoural radiopeptide therapy.

Methods For test and therapeutic injections, 2 MBq of ^{111}In-substance P and 370–3,330 MBq of ^{90}Y-substance P, respectively, were applied in 12 patients with malignant gliomas. Over a period of 24 h, serial SPECT scans were performed on a dual-head SPECT camera. The scans were acquired in a double-energy window technique together with ^{99m}Tc-ECD in order to co-register the dose distributions with a separately acquired, contrast-enhanced CT scan. Quantitative voxelwise dose distribution maps (in Gy/GBq) were computed from these data using a mono-exponential decay approach. Pre- and post-therapeutic values were compared.
Results Agreement between pre- and post-therapeutic dosimetry was very good and delivered absolute dose values in Gy per injected GBq. In all patients, the pretherapeutic test injection together with the CT overlay technique could predict the precise localisation of dose deposition in an anatomical context.
Conclusion This protocol allows a precise pretherapeutic computation of the expected three-dimensional dose distribution and is clearly superior to the previously used dosimetry based on planar scintigraphic images. It has become an indispensable tool for planning intratumoural radiopeptide therapy in glioma patients.

Keywords Substance P · Malignant glioma · Targeted radiotherapy · Dosimetry · NK-1 receptors

S. Kneifel (✉) · J. Müller-Brand
Clinic and Institute for Nuclear Medicine,
University Hospital Basel,
Basel, Switzerland
e-mail: skneifel@uhbs.ch

P. Bernhardt · H. Uusijärvi
Department of Radiation Physics, University of Göteborg,
Göteborg, Sweden

S. Good · H. Mäcke
Division of Radiological Chemistry, University Hospital Basel,
Basel, Switzerland

L. Plasswilm
Institute for Radiation Oncology, University Hospital Basel,
Basel, Switzerland

C. Buitrago-Téllez
Institute for Diagnostic Radiology, University Hospital Basel,
Basel, Switzerland

A. Merlo
Clinic for Neurosurgery, University Hospital Basel,
Basel, Switzerland

Introduction

For targeted radiotherapy, we have developed a protocol for malignant gliomas using the radiolabelled somatostatin analogue ^{90}Y-DOTATOC [1] for local intratumoural injec-

tion. First promising results have been obtained [2]. A drawback of this targeting system is the inconsistent expression of somatostatin receptors, especially in prevalent glioblastoma. However, neurokinin type 1 (NK-1) receptors, which can be targeted with their native ligand substance P [3], are consistently overexpressed in all malignant gliomas [4], including glioblastomas. We have constructed a peptidic vector consisting of the natural sequence of substance P, which is conjugated with DOTAGA, a chelator for metallic radionuclides [5, 6]. The β emitter ^{90}Y was used for therapy, and the γ emitter ^{111}In for diagnostic test injections. First clinical results are encouraging and have been published recently [7]; only transient local toxicity (radiogenic oedema) was seen as a side-effect, whereas neurological improvement could be observed in 65% of the patients.

An accurate method to calculate tumour dose is required in order to correlate the deposited energy with clinical response. Geometrical tumour models, at present mostly used for dose estimation, depend upon the assumption of a simple, non-biological three-dimensional tumour geometry, enhancing small one-dimensional inaccuracies to large error ranges [8–10]. Inhomogeneous biodistribution of the radiopharmaceutical and inconstant biological half-lives further limit the reliability of dose estimates based on such models. Dosimetry based on planar scintigraphic images and tumour volumetries derived from MRI has proven to be unsatisfactory owing to large error ranges of at least ±20% [1].

In order to overcome these limitations, we have developed a new method to compute individual in vivo doses based on SPECT measurements to account for variance in activity distribution and biological half-life of the radiopharmaceutical. The aim of the present study was to implement a dosimetry protocol that allows accurate assessment of the dose using the diagnostic radionuclide ^{111}In prior to the actual therapeutic administration of ^{90}Y-labelled substance P.

Mathematical background

We assumed that the pharmacokinetics of radiolabelled substance P follows a mono-exponential decay model. Thus the activity concentration dependent on the location and the time t can be described by the following equation:

$$C(x,y,z,t) = C(x,y,z,0) \cdot e^{-\lambda t} \tag{1}$$

with $C(x, y, z, t)$ denoting the activity concentration dependent on three spatial coordinates x, y, z and the time t, and λ denoting the effective decay constant, consisting of its two components λ_{phys} (physical half life, equal to $\ln 2/T_{half\text{-}life}$) and λ_{biol} (biological half-life):

$$\lambda = \lambda_{phys} + \lambda_{biol} \tag{2}$$

Equation (1) can be written in logarithmic form:

$$\ln C(x,y,z,t) = \ln C(x,y,z,0) - \lambda t \tag{3}$$

from which the effective decay constant λ for each voxel element can be estimated from the three measurement points $C(x,y,z,t)$ by linear regression analysis.

In the evaluation of pretherapeutic SPECT measurements, the activity concentration of ^{90}Y was estimated from ^{111}In measurements by half-life correction:

$$C_Y(x,y,z,t) = C_{\ln}(x,y,z,t) \cdot e^{\left(\lambda_{phys(In)} - \lambda_{phys(Y)}\right)\cdot t} \tag{4}$$

where $\lambda_{phys(In)}$ denotes the physical decay constant for ^{111}In and $\lambda_{phys(Y)}$ the physical decay constant for ^{90}Y.

The absorbed energy dose to a voxel can be obtained from Eq. 1 by integrating over the concentration from injection time until infinity:

$$D(x,y,z) = k\int_0^{+\infty} C(x,y,z,0)e^{-\lambda t}dt = \frac{k}{\lambda}C(x,y,z,0) \tag{5}$$

with k denoting a constant based on the assumption of a local energy deposition of 930.8 keV (i.e. the medium energy deposition per ^{90}Y decay).

We deliberately abstained from using Monte Carlo simulation for the computation of dose deposition and assumed a local energy deposition for β decay events. We computed the dose kernel of a ^{90}Y point source in water using PENELOPE [11, 12] and got a full-width at half-maximum (FWHM) of 3 mm (Fig. 1). Since by SPECT scanning the true activity distribution is convoluted by a point spread function with a surely larger FWHM, the acquired activity distributions are already blurred, compared with the true tissue distribution. As Monte Carlo simulation can be approximated with dose kernels in a first approximation, it would only enlarge the resulting convolution kernel. Therefore, we decided to omit Monte Carlo procedures and to assume a local decay.

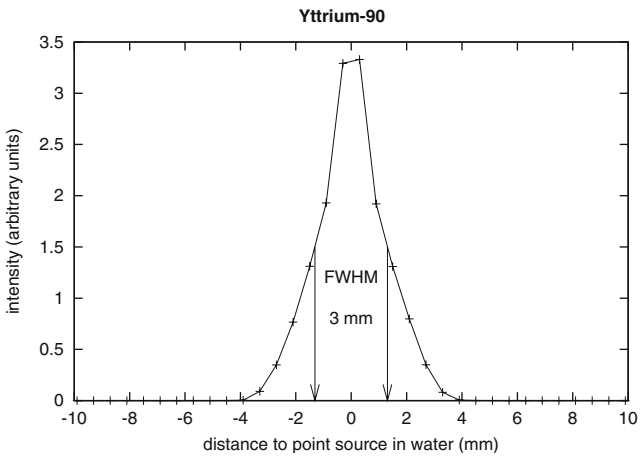

Fig. 1 Dose kernel of a ^{90}Y point source in water

Materials and methods

Twelve glioma patients, nine of male and three of female gender, with a mean age of 47 years (range 31–64), were included in a targeted radiotherapy study protocol or treated accordingly [7]. The protocol was compliant with the Helsinki Declaration and had been approved by the local Ethics Committee. All patients gave their informed consent. The following tumour histologies were included for dosimetry: four glioblastomas (WHO grade IV), two anaplastic gliomas (WHO grade III) and six low-grade astrocytomas (WHO grade II). In all patients, the diagnosis was proven by stereotactic biopsy. Following biopsy, a ventricular catheter, connected to a subcutaneous cerebrospinal fluid reservoir, was inserted into the tumour mass.

Radiopeptide chemistry

The peptide was assembled on solid phase with a semi-automatic peptide synthesiser (RinkCombichem Technologies, Bubendorf, Switzerland) using fluorenylmethoxycarbonyl-polyamide solid phase peptide synthesis [13]. DOTAGA $(tBu)_4$ was introduced as a protected prochelator at the N-terminal end of the undecapeptide [14]. After deprotection and purification using reversed phase high-performance liquid chromatography (RP-HPLC; Bischoff HPLC system, Metrohm AG, Herisau, Switzerland), the chelator–peptide conjugate was obtained in high purity (>95%). Identity was confirmed by MALDI-TOF mass spectroscopy (Voyager-DE STR, Applied Biosystems, Framingham, MA, USA). The chelator–peptide conjugate was labelled with a specific activity of 67.3 MBq/pmol of ^{90}Y for therapeutic studies. For diagnostic purposes, 2 MBq of ^{111}In was used per application. The chelator–peptide conjugate was dissolved in 500 μl sterile filtered buffer containing 16.4 mg sodium acetate, 18.5 mg (2,5)-dihydroxybenzoic acid and 0.1 g of L (+)-ascorbic acid sodium salt. The radiometal was added and incubated for 30 min at 95°C. Quality control was performed using RP-HPLC (Macherey-Nagel CC 250/4 Nucleosil 120-3 C18, flow: 0.75 ml/min, eluents: A=acetonitrile, B=0.1% trifluoroacetic acid in water; gradient: 0 min, 95% B; 30 min, 55% B; 32 min, 0% B; 34 min, 0% B; 37 min, 95% B; retention time 23 min). A radiochemical purity of more than 99% for ^{90}Y and more than 90% for ^{111}In was achieved. For injection, the solution was prepared by dilution with 0.9% NaCl solution to a volume of 1 ml.

Imaging techniques

We performed pretherapeutic dosimetry using 2 MBq of ^{111}In-labelled substance P in every patient, followed by one to four therapeutic injections of 370–3,330 MBq ^{90}Y-labelled substance P, depending on tumour size and biodistribution aspects such as proximity to functionally critical areas. Time between test injection and first therapy cycle was 1 week. Other cycles followed with a time distance of normally 2 weeks, which was adapted if clinical symptoms required it. For anatomical correlation of SPECT measurements, we co-injected 500 MBq of the brain perfusion marker ^{99m}Tc-*N*,*N*′-1,2-ethylenediylbis-L-cysteine diethyl ester hydrochloride (^{99m}Tc-ECD=^{99m}Tc-bicisate; Neurolite, Bristol-Myers Squibb, Massachusetts, USA) [15–17]. We performed SPECT scans, carefully preserving the head position relative to the scanner, at three different time points: the first immediately after the injection, the second 3–5 h p.i. and the third 21–24 h p.i. This was a compromise between a possibly more refined dosimetry using a bi-exponential approach, which would require at least four time points, and the need for a simple and pragmatic protocol which does not overtax patients and fits into a busy clinical routine. Scanning duration was 30 min, using continuous acquisition (6° per minute) on a dual-head γ camera (Picker P 2000, Philips Medical Systems, Eindhoven, The Netherlands), which was calibrated and tested for linearity according to local and national quality control guidelines. The scans were acquired with a medium-energy collimator in multiple energy windows in order to distinguish ^{99m}Tc from either ^{111}In or ^{90}Y. For pretherapeutic dosimetry with ^{111}In, three energy windows were used: 140 keV (±7.5%) for ^{99m}Tc, and 171 keV (±10%) and 245 keV (±10%) for ^{111}In. For dosimetry after the therapeutic injections, two energy windows were used: the ^{99m}Tc window was kept at 140 keV, whereas a larger continuum window at 306 keV (±45%) was used to detect ^{90}Y bremsstrahlung owing to its low count rate. Images were reconstructed iteratively (maximum likelihood expectation minimisation, 20 iterations [18]), filtered with a low-pass filter (order 4.0, cutoff frequency 0.26/pixel) and finally corrected for attenuation (coefficients: 0.110/cm for ^{99m}Tc and 0.090/cm for ^{90}Y/^{111}In). Attenuation correction was performed by defining elliptical regions covering the whole brain on ^{99m}Tc images; the ellipses were then transformed to the co-registered ^{90}Y/^{111}In images and applied as correction templates. Reconstructed images had a voxel size of $4.67 \cdot 4.67 \cdot 4.67$ mm^3. No scatter correction was used, as the algorithms described in the literature are designed for γ-emitting nuclides and not for bremsstrahlung imaging [19–23]. Voxels with less than 5% of the maximum voxel value were masked out in order to correct for noise far away from the tumour, which could influence the computation of the initial activity distribution immediately after radiopeptide administration. An example for the resulting distributions images is given in Fig. 2.

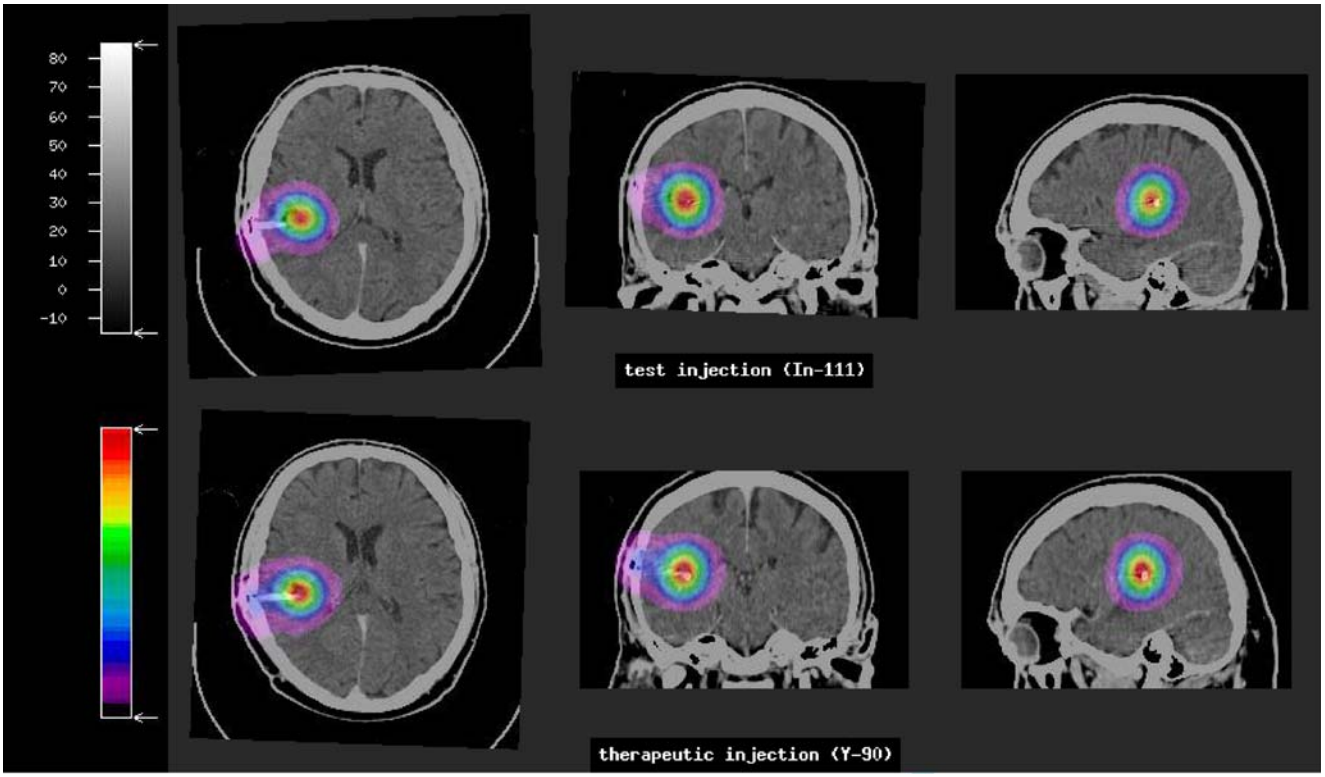

Fig. 2 Bremsstrahlung imaging with ^{90}Y. Following local injection, similar biodistribution can be visualised as compared to test injection with ^{111}In

Data processing

We performed manual image fusion using dedicated image fusion software (MPI-Tool, Advanced Tomo Vision GmbH, Kerpen, Germany [24, 25]). Outlines of the ^{99m}Tc-ECD image were projected onto a diagnostic contrast-enhanced CT scan, and rotation/translation parameters were adapted until the match between the two modalities was satisfactory. Then, the rotation and translation parameters of the ^{99m}Tc-ECD image were applied to the co-acquired ^{111}In/^{90}Y images. For each voxel of the resliced images, a linear regression analysis between the time after administration as the independent variable and the natural logarithm of the count rates as the dependent variable was calculated. The resulting slope and intercept values were stored voxel by voxel into separate files S and I. λ and $C(x,y,z,0)$ were then calculated:

$$\lambda(x,y,z) = S(x,y,z) \tag{6}$$

$$C(x,y,z,0) \sim e^{I(x,y,z)} \tag{7}$$

$$\sum_x \sum_y \sum_z C(x,y,z,0) = A_{\text{total}} \tag{8}$$

assuming that at injection time (i.e. $t=0$) the whole locally injected activity A_{total} was contained in the volume of visible accumulation in the SPECT images, which was defined as the set of all voxels whose count rate exceeded 5% of the maximum count rate of the total acquired volume. The sum of all voxels in this set was assumed to correspond to the total administered activity. Further acquisitions were performed with the same patient and camera positions as the first scan, thus assuming linearity between the several scans of one patient's series. The cameras had been checked before for linearity according to the manufacturer's recommendations; it was assured that no recalibration procedure took place between the scans. Analytic integration of the fitted time-activity curves between $t=0$ and $t=+\infty$ yielded the cumulative number of decay events per voxel. Assuming an average energy deposition of 930.8 keV per ^{90}Y β decay and a specific gravity of 1.0 g/cm^3 for the absorbing tissue, we calculated quantitative dose distribution maps in Gy. The tumour region was identified on the co-registered SPECT and CT images, and the maximum voxel values of pre- and post-therapeutic dose maps (in Gy per injected GBq) were correlated.

Results

Logarithmic fitting was successful in all patients, yielding quantitative voxelwise parametric maps of dose distribution

which could be projected to the contrast-enhanced CT scan. The correct deposition of the maximum dose into the tumour could be documented at all pretherapeutic test injections. An example is given in Fig. 3.

Computed maximum doses at the test injection ranged from 74 to 505 Gy/GBq with a mean dose of 199 Gy/GBq. The doses computed at the time of therapeutic injection ranged from 12 to 483 Gy/GBq and decreased from injection to injection over time in the majority of cases. The dosimetric results as well as the injected activities are given in detail in Table 1.

A comparison between pretherapeutic and the first post-therapeutic dosimetry yielded conforming results in nearly all cases (Fig. 4; dotted line, $r^2=0.79$). In this series of patients we had included two cases with suboptimal biodistribution (patient no. 8) or an incidentally higher ^{111}In activity (patient no. 9). While this reflects clinical reality, upon subtraction of these two cases, an even better correlation was obtained in the residual ten patients ($r^2=0.89$; solid line in Fig. 4).

Discussion

This novel dosimetry protocol for local therapy of brain tumours is feasible and highly reproducible. Planar scintigraphic images cannot ascertain the exact localisation of the therapeutic activity within the tumour borders. In contrast, the presented method allows precise visualisation of the expected quantitative dose distribution in relation to tumour geometry and adjacent brain tissue. Patients not suited for locally targeted radiopeptide therapy due to unfavourable biodistribution can therefore be excluded following test injection with ^{111}In.

Other groups have recently tried different approaches to quantify the dose delivered to the target. Ferrari et al. [10] used Monte Carlo methods to compute S values from a virtual phantom and applied these to patients. However, this does not account for distribution inhomogeneities between different regions of the same tumour. They estimated transit times and hence clearance from urine measurements; while this is probably a good estimator of an overall averaged clearance, regional differences could occur owing to inhomogeneous receptor density and inhomogeneous vitality of tumour cells. Akabani et al. [8] used direct measurements using a probe placed externally over the surgical resection cavity. This might give a better estimation of effective half-life in loco; however, this likewise does not account for regional differences. In our experience, often several catheters are needed to guarantee a similar dose deposition throughout the tumour; judging where these additional catheters should be placed is not possible using geometric models or global decay measurements.

Some possible error sources need to be discussed:

Different physical properties of radionuclides One may suspect that different physical properties of the two radionuclides could introduce errors considering possible scatter and attenuation artefacts. This aspect probably does not affect the measurement of effective half-life times, as these effects can be expected to be similar among several scans and not to impair linearity. It could affect the measured radiopharmaceutical distribution, with a faulty attribution of activity to voxels without actual irradiation sources. Masking out voxels without a reasonable probability of radionuclide accumulation is therefore necessary, as described in the Materials and methods section. Scatter correction algorithms have been suggested to deal with this problem [19–23]. However, these algorithms were developed for γ-emitting nuclides, not for imaging of bremsstrahlung. When we tried to apply these algorithms, we obtained non-evaluable activity distribution images. One might argue that

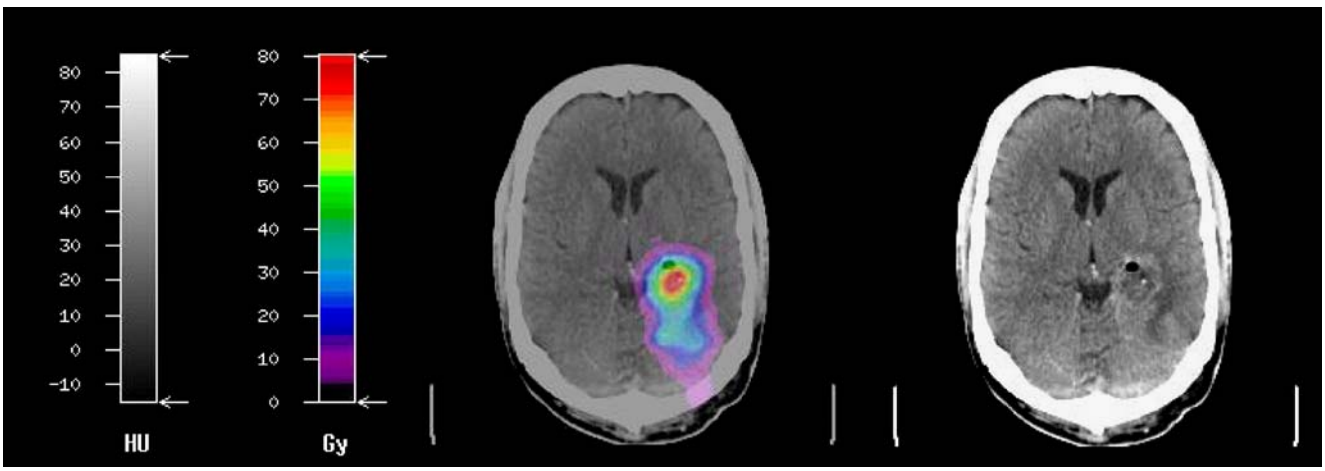

Fig. 3 Quantitative voxelwise dose map in a patient with glioblastoma multiforme documenting an orthotopic dose distribution

Table 1 Dosimetry results in Gy/GBq

Patient no.	Sex	Age (yr)	Diagnostic ^{111}In	Therapy 1 ^{90}Y	Therapy 2 ^{90}Y	Therapy 3 ^{90}Y	Therapy 4 ^{90}Y
1	m	42	204	67 74 Gy/1.11 GBq	81 150 Gy/1.85 GBq	–	–
2	m	46	88	84 93 Gy/1.11 GBq	60 66 Gy/1.11 GBq	55 121 Gy/2.22 GBq	–
3	m	56	88	79 88 Gy/1.11 GBq	–	–	–
4	m	50	74	56 124 Gy/2.22 GBq	51 151 Gy/2.96 GBq	–	–
5	m	31	223	226 251 Gy/1.11 GBq	269 298 Gy/1.11 GBq	–	–
6	f	42	249	198 220 Gy/1.11 GBq	79 88 Gy/1.11 GBq	38 42 Gy/1.11 GBq	12 14 Gy/1.11 GBq
7	m	47	75	59 65 Gy/1.11 GBq	48 160 Gy/3.33 GBq	87 291 Gy/3.33 GBq	102 341 Gy/3.33 GBq
8	f	53	131	40 44 Gy/1.11 GBq	–	–	–
9	m	64	505	308 114 Gy/0.37 GBq	355 394 Gy/1.11 GBq	–	–
10	f	46	118	109 241 Gy/2.22 GBq	143 317 Gy/2.22 GBq	–	–
11	m	44	456	483 198 Gy/0.41 GBq	304 170 Gy/0.56 GBq	–	–
12	m	37	176	146 175 Gy/1.20 GBq	207 230 Gy/1.11 GBq	103 114 Gy/1.11 GBq	–

– denotes not performed

the wide range of absolute doses might be due to inaccuracies in acquisition or processing of the data; however, the good correlation between ^{111}In and ^{90}Y ($p<0.01$) with their different physical properties makes this hypothesis unlikely and supports the use of the approach discussed in this report.

Different distribution volumes If the tumour is growing rapidly, the dosimetry may be inaccurate owing to different distribution volumes of the radiopharmaceutical, especially if the tumour is gaining access to open cerebrospinal fluid (CSF) spaces. Considering the fact that an increase in the distribution volume leads to a decrease in the deposited energy per mass unit (= Gy), the dose would be over- rather than underestimated. In such cases, additional injections may be needed to reach the intended dose in the target area. However, if the outflow of the radiopharmaceutical into the CSF spaces is excessive and no specific tumour uptake can be visualised on SPECT images, further treatments should not be applied.

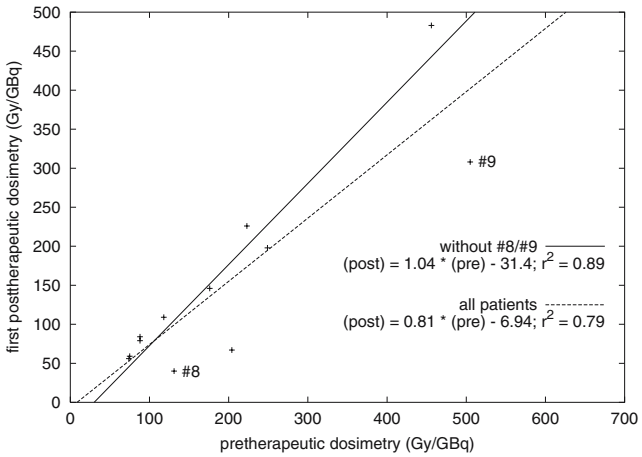

Fig. 4 Comparison between diagnostic and first therapeutic dosimetry (*dotted line*, all patients; *solid line*, after exclusion of patients 8 and 9)

Possible count loss at high count rates This might have happened in patient no. 9: a higher amount of ^{111}In (5 MBq) was incidentally administered at test injection into a relatively small tumour volume (2 ml). Compared with the dosimetry at the first therapy cycle, the dose was computed substantially higher. It is not clear whether this is within the fluctuation margin of the method; however, a possible count loss at high count rates might have played a role. In such a case, the decay curve gets more shallow, leading to an underestimation of λ in Eq. 3 and an overestimation of $D(x,y,z)$ according to Eq. 5. In practice, this could lead to a reduction in the prescribed ^{90}Y activity and consequently to undertreatment of the tumour.

One might argue that the comparison of maximum doses could be inaccurate owing to local inequalities in dose distribution and that a correlation of medium doses or dose–volume histograms might be a more adequate method. Unfortunately, even on contrast-enhanced CT, especially low-grade gliomas are often not clearly delimitable from the surrounding tissue, as could be observed in comparison to positron emission tomography using proliferation markers [26]. This makes the definition of exact tumour borders very difficult and would therefore probably introduce an additional error source. The maximum dose value was therefore chosen as a more robust estimator. Owing to the limited resolution of the acquisition and reconstruction processes, images are likewise convoluted by a smoothing kernel; thus, the potential influence of single deviating voxels is minimised.

The clinical meaning of the computed doses remains to be defined. In vivo validation of the method by absolute dose values is not practicable, because this would require implantation of dosimeters into the brain of patients. Assuming an average administered activity of around 1 GBq, doses vary between ten and several hundred grays owing to variations in biological half-life of the radiopharmaceutical at the tumour site. However, the dose rate is much lower than in conventional external beam radiotherapy or conforming irradiation techniques. Typically, with external beam irradiation a dose of about 2 Gy is administered in 20–30 s (corresponding to about 0.1 Gy/s). Targeted radiopeptide therapy delivers its dose over a much longer period, resulting in a lower dose rate (by about one to two orders of magnitude). This results in fewer ionising events per time unit, and DNA damage in tumour cells is likely to be more efficiently repaired during low-dose-rate brachytherapy than in conventional high-dose-rate external beam radiotherapy.

A well-known example in the field of radiation oncology is permanent ^{125}I or ^{103}Pd seed implantation for the treatment of early prostate cancer. Using ^{125}I seeds, the most commonly prescribed dose is 160 Gy, and the minimal dose to 90% of the outlined prostate volume should be equal to or greater than 145 Gy [27–30]. In contrast, external beam radiation is typically performed with a total dose of about 72–74 Gy with daily fractions of 2 Gy.

Malignant gliomas are among the most radioresistant tumours; even 90 Gy externally applied radiation dose is not sufficient to sterilise glioblastoma multiforme in vivo [31]. Therefore the doses of several hundred grays administered by ^{90}Y radiopeptide therapy computed in this study lay within a reasonable order of magnitude, assuming a multiplicator of at least 2–3 of the doses applied in conventional external beam radiotherapy.

Most patients showed a decreasing dose deposition from injection to injection over time, caused by shortening of biological half-lives. The reason for this is not yet clear. Repetitive therapies may reduce viable tumour cells and their binding sites for substance P. Another possibility is an increase in the blood-brain barrier permeability following radiation damage of endothelial cells, resulting in a greater loss of substance P into the systemic circulation.

Two patients (nos. 5 and 7) showed a sudden increase in retention time and dose per administered activity. This coincided with a reduction in CT tumour density to below 20 Hounsfield units (HU), suggesting necrotic transformation of the tumour. A loss of draining vessels may be the critical factor for this effect.

The approach can be further improved by the use of a dedicated SPECT/CT device to eliminate the need for co-injection of ^{99m}Tc-ECD, which may cause an error due to approximative attenuation correction and manual image fusion.

In order to correlate computed doses with toxicity, which mainly consists of perifocal radiation necrosis, and to define therapeutic doses, a follow-up study will be initiated to further develop this novel treatment modality.

Acknowledgements The authors thank our technical, laboratory and medical staff for their professional support in preparing the radiopharmaceuticals as well as in acquiring SPECT scans and preparing the patients for injections. The study was supported by the Swiss National Science Foundation, Tandem program, grant #3238-056368.99/1 and its extension #3238-069472/2 (to A.M.). Additional support was obtained from the Research Fund of the Surgical Department of the University Hospital of Basel.

References

1. Merlo A, Hausmann O, Wasner M, Steiner P, Otte A, Jermann E, et al. Locoregional regulatory peptide receptor targeting with the diffusible somatostatin analogue ^{90}Y-labeled DOTA^{0}-D-Phe^{1}-Tyr^{3}-octreotide (DOTATOC): a pilot study in human gliomas. Clin Cancer Res 1999;5:1025–33.
2. Schumacher T, Hofer S, Eichhorn K, Wasner M, Zimmerer S, Freitag P, et al. Local injection of the ^{90}Y-labelled peptidic vector DOTATOC to control gliomas of WHO grades II and III: an extended pilot study. Eur J Nucl Med Mol Imaging 2002;29:486–93.
3. Reubi JC. Peptide receptors as molecular targets for cancer diagnosis and therapy. Endocr Rev 2003;24:389–427.
4. Hennig IM, Laissue JA, Horisberger U, Reubi JC. Substance-P receptors in human primary neoplasms: tumoral and vascular localization. Int J Cancer 1995;61:786–92.
5. Eisenwiener KP, Powell P, Mäcke HR. A convenient synthesis of novel bifunctional prochelators for coupling to bioactive peptides for radiometal labelling. Bioorg Med Chem Lett 2000;10:2133–5.
6. Mäcke HR, Good S. Radiometals (non-Tc, non-Re) and bifunctional labeling chemistry. In: Vértes A, Nagy S, Klencsár Z, editors. Handbook of nuclear chemistry. Amsterdam: Kluwer Academic; 2004. pp. 279–314.
7. Kneifel S, Cordier D, Good S, Ionescu MC, Ghaffari A, Hofer S, et al. Local targeting of malignant gliomas by the diffusible peptidic

vector 1,4,7,10-tetraazacyclododecane-1-glutaric acid-4,7,10-triacetic acid-substance P. Clin Cancer Res 2006;12:3843–50.
8. Akabani G, Reist CJ, Cokgor I, Friedman AH, Friedman HS, Coleman RE, et al. Dosimetry of ^{131}I-labeled 81C6 monoclonal antibody administered into surgically created resection cavities in patients with malignant brain tumors. J Nucl Med 1999;40:631–8.
9. Akabani G, Cokgor I, Coleman RE, González Trotter D, Wong TZ, Friedman HS, et al. Dosimetry and dose-response relationships in newly diagnosed patients with malignant gliomas treated with ^{131}I-labeled anti-tenascin monoclonal antibody 81C6 therapy. Int J Radiat Oncol Biol Phys 2000;46:947–58.
10. Ferrari M, Cremonesi M, Bartolomei M, Bodei L, Chinol M, Fiorenza M, et al. Dosimetric model for locoregional treatments of brain tumors with ^{90}Y-conjugates: clinical application with ^{90}Y-DOTATOC. J Nucl Med 2006;47:105–12.
11. Stewart RD, Wilson WE, McDonald JC, Strom DJ. Microdosimetric properties of ionizing electrons in water: a test of the PENELOPE code system. Phys Med Biol 2002;47:79–88.
12. Ye SJ, Brezovich IA, Pareek P, Naqvi SA. Benchmark of PENELOPE code for low-energy photon transport: dose comparisons with MCNP4 and EGS4. Phys Med Biol 2004;49:387–97.
13. Atherton E, Sheppard RC. Fluorenylmethoxycarbonylpolyamide solid phase peptide synthesis: general principles and development. In: Solid phase peptide synthesis: a practical approach. Eynsham, Oxford: IRL Press; 1989. pp. 25–37.
14. Heppeler A, Froidevaux S, Mäcke HR, Jermann E, Béhé M, Powell P, et al. Radiometal-labelled macrocyclic chelator-derivatised somatostatin analogue with superb tumour-targeting properties and potential for receptor-mediated internal radiotherapy. Chem Eur J 1999;5:1974–81.
15. Vallabhajosula S, Zimmerman RE, Picard M, Stritzke P, Mena I, Hellman RS, et al. ^{99m}Tc ECD: a new brain imaging agent: in vivo kinetics and biodistribution studies in normal human subjects. J Nucl Med 1989;30:599–604.
16. Léveillé J, Demonceau G, De Roo M, Rigo P, Taillefer R, Morgan RA, et al. Characterization of ^{99m}Tc-L,L-ECD for brain perfusion imaging, part 2: biodistribution and brain imaging in humans. J Nucl Med 1989;30:1902–10.
17. Holman BL, Hellman RS, Goldsmith SJ, Mena IG, Leveille J, Gherardi PG, et al. Biodistribution, dosimetry, and clinical evaluation of ^{99m}Tc ethyl cysteinate dimer in normal subjects and in patients with chronic cerebral infarction. J Nucl Med 1989;30:1018–24.
18. Shepp LA, Vardi Y. Maximum likelihood reconstruction for emission tomography. IEEE Trans Med Imaging 1982;1:113–22.
19. Barnden LR, Hatton RL, Behin-Ain S, Hutton BF, Goble EA. Optimisation of brain SPET and portability of normal databases. Eur J Nucl Med Mol Imaging 2004;31:378–87.
20. Kim KM, Varrone A, Watabe H, Shidahara M, Fujita M, Innis RB, et al. Contribution of scatter and attenuation compensation to SPECT images of nonuniformly distributed brain activities. J Nucl Med 2003;44:512–9.
21. Larsson A, Johansson L, Sundström T, Ahlström KR. A method for attenuation and scatter correction of brain SPECT based on computed tomography images. Nucl Med Commun 2003;24:411–20.
22. Shidahara M, Watabe H, Kim KM, Kato T, Kawatsu S, Kato R, et al. Development of a practical image-based scatter correction method for brain perfusion SPECT: comparison with the TEW method. Eur J Nucl Med Mol Imaging 2005;32:1193–8.
23. Vines DC, Ichise M, Liow JS, Toyama H, Innis RB. Evaluation of 2 scatter correction methods using a striatal phantom for quantitative brain SPECT. J Nucl Med Technol 2003;31:157–60.
24. Pietrzyk U, Herholz K, Heiss WD. Three-dimensional alignment of functional and morphological tomograms. J Comput Assist Tomogr 1990;14:51–9.
25. Pietrzyk U, Herholz K, Schuster A, von Stockhausen HM, Lucht H, Heiss WD. Clinical applications of registration and fusion of multimodality brain images from PET, SPECT, CT, and MRI. Eur J Radiol 1996;21:174–82.
26. Herholz K, Hölzer T, Bauer B, Schröder R, Voges J, Ernestus RI, et al. ^{11}C-methionine PET for differential diagnosis of low-grade gliomas. Neurology 1998;50:1316–22.
27. Ling CC. Permanent implants using ^{198}Au, ^{103}Pd and ^{125}I: radiobiological considerations based on the linear quadratic model. Int J Radiat Oncol Biol Phys 1992;23:81–7.
28. Nath R, Anderson LL, Luxton G, Weaver KA, Williamson JF, Meigooni AS. Dosimetry of interstitial brachytherapy sources: recommendations of the AAPM (American Association of Physicists in Medicine) Radiation Therapy Committee Task Group No. 43. Med Phys 1995;22:209–34.
29. Prete JJ, Prestidge BR, Bice WS, Friedland JL, Stock RG, Grimm PD. A survey of physics and dosimetry practice of permanent prostate brachytherapy in the United States. Int J Radiat Oncol Biol Phys 1998;40:1001–5.
30. Nag S, Beyer D, Friedland J, Grimm P, Nath R. American Brachytherapy Society (ABS) recommendations for transperineal permanent brachytherapy of prostate cancer. Int J Radiat Oncol Biol Phys 1999;44:789–99.
31. Chan JL, Lee SW, Fraass BA, Normolle DP, Greenberg HS, Junck LR, et al. Survival and failure patterns of high-grade gliomas after three-dimensional conformal radiotherapy. J Clin Oncol 2002;20:1635–42.